J Solid State Electrochem (2012) 16:2805–2813
DOI 10.1007/s10008-012-1705-8

ORIGINAL PAPER

Effects of carbon sources and carbon contents on the electrochemical properties of $LiFePO_4$/C cathode material

Kerun Yang · Zhenghua Deng · Jishuan Suo

Received: 8 October 2011 / Revised: 20 February 2012 / Accepted: 23 February 2012 / Published online: 8 March 2012

Abstract $LiFePO_4$/C composites are prepared by using two types of carbon source: one using polymer (PAALi) and the other using sucrose. The physical characteristics of $LiFePO_4$/C composites are investigated by X-ray diffraction), scanning electron microscopy, BET, laser particle analyzer, and Raman spectroscopy. Their electrochemical properties are characterized by cyclic voltammograms, constant current charge–discharge, and electrochemical impedance spectra. These analyses indicate that the carbon source and carbon content have a great effect on the physical and electrochemical performances of $LiFePO_4$/C composites. An ideal carbon source and appropriate carbon content can effectively increase the lithium-ion diffusion coefficient and exchange current density, decrease the charge transfer resistance (R_{ct}), and enhance the electrochemical performances of $LiFePO_4$/C composite. The results show that PAALi is a better carbon source for the synthesis of $LiFePO_4$/C composites. When the carbon content is 4.11 wt.% (the molar ratio of PAALi/$Li_2C_2O_4$ was 2:1), as-prepared $LiFePO_4$/C composite shows the best combination between electrochemical performances and tap density.

Keywords Lithium iron phosphate · Carbon source · Carbon content

K. Yang · Z. Deng · J. Suo
Chengdu Institute of Organic Chemistry,
Chinese Academy of Sciences,
Chengdu, Sichuan 610041, People's Republic of China

K. Yang · Z. Deng (✉) · J. Suo
Graduate School of Chinese Academy of Sciences,
Beijing 100039, People's Republic of China
e-mail: zhdeng@cioc.ac.cn

Introduction

Olivine-type $LiFePO_4$ was first reported by Good-enough's group in 1997 [1] as a potential cathode material for lithium-based secondary batteries because of its numerous appealing features, such as high theoretical capacity of 170 mAh g^{-1} [2–4], high safety [5–9], low cost [10–12] and environmental friendliness [13, 14]. However, $LiFePO_4$ suffers from low ionic transport rate, low electronic conductivity, low tap density, and poor batch reproducibility. In order to enhance the electronic conductivity and electrochemical properties of $LiFePO_4$ cathode materials, tremendous efforts have been made, which include: (1) doping $LiFePO_4$ with foreign atoms [15–17]. Though this method can increase the conductivity to some degree [16], introducing guest atoms into the crystal lattices of $LiFePO_4$ may also be deleterious if it occurs on the lithium sites [18]; (2) surface coating or admixing with electronically conductive materials (carbon [19–24] and conducting polymers [25–28]) has also been studied; (iii) decreasing the particle size may also improve the ionic transport issues [29–31]. Reducing the particle size can significantly shorten the diffusion time of Li in $LiFePO_4$, resulting in a much enhanced power performance. From the above-mentioned technologies, surface carbon coating has been widely used for improving the electronic conductivity of $LiFePO_4$. However, carbon sources and carbon contents are the most important influence factors on the electrochemical performances of $LiFePO_4$/C.

In a previous work, many materials were used as carbon sources, such as glucose, sucrose, oxalic acid, polystyrene, polyvinyl alcohol, and so on. To conclude, these materials are either polymer or low molecular weight organic matter. In this paper, two types of carbon source were employed to prepare $LiFePO_4$/C composite: one using polymer (PAALi), the other using low molecular weight organic matter

(sucrose). The effects of carbon sources on the physical structure and electrochemical properties of $LiFePO_4$/C composite were systematically studied and compared. Furthermore, the effects of carbon contents on the tap density and electrochemical properties of $LiFePO_4$/C composite were also investigated in detail.

Experimental

Synthesis of the $LiFePO_4$/C composite

$LiFePO_4$/C derived from different carbon sources

$FePO_4 \cdot 2H_2O$, $Li_2C_2O_4$, and PAALi (PAALi/$Li_2C_2O_4$=2:1, according to the molar ratio) were dissolved in de-ionized water, and then a small quantity of $H_2C_2O_4 \cdot 2H_2O$ was added to the solutions to adjust the system to neutrality or slight acidity (pH=5–7). The above-mentioned solution was thoroughly mixed by ball-milling in a planetary QM-3SP2 mill for 6 h. The homogeneous slurry was dried at 120 °C for 6 h to obtain the precursor. For comparison, the other precursor was prepared by using sucrose instead of PAALi. The $LiFePO_4$/C powder was synthesized in two steps: the said precursors were first decomposed at 500 °C for 2 h and then sintered at 700 °C for 15 h. The samples were denoted as LFP-A and LFP-B, respectively. Decomposing and sintering were both carried out in flowing N_2 atmosphere.

$LiFePO_4$/C with different carbon contents using different molar ratios of LiPAA and $Li_2C_2O_4$

Different molar ratios of organic lithium sources (LiPAA and $Li_2C_2O_4$), $FePO_4 \cdot 2H_2O$, and $H_2C_2O_4 \cdot 2H_2O$ were thoroughly mixed by ball-milling in a planetary QM-3SP2 mill for 6 h. The homogeneous slurries were dried at 120 °C for 6 h to obtain the precursors. Subsequently, the said precursors were first decomposed at 500 °C for 2 h and then sintered at 700 °C for 15 h. The samples were denoted as LFP-A_1, LFP-A_2, LFP-A_3, LFP-A_4, LFP-A_5, LFP-A_6, LFP-A_7, and LFP-A_8, respectively, which were listed in Table 6.

Characterization of the precursor and $LiFePO_4$/C composite

The crystallographic structural characterization was performed by X-ray powder diffraction (XRD). XRD of the $LiFePO_4$/C composites was carried out on a Philips X′ Pert diffractometer equipped with Cu-$K\alpha$ radiation of λ= 0.15418 nm in the range of $15^o<2\theta<80^o$. The micromorphology of the precursors and $LiFePO_4$/C composites was observed using an Impect F (FEI Company) scanning electron microscopy. The surface carbon structure in the samples was investigated by Raman spectroscopy (Invia Raman Microscope), with an excitation wavelength of 325 nm. The particle size ($D50$) of the $LiFePO_4$/C composites was obtained from BT-9300H laser particle analyzer. The specific surface area was measured by nitrogen adsorption/desorption at −196 °C using a Builder SSA-4200 apparatus, and carbon content was detected using a CARLO ERBA 1106 elemental analyzer (Italy).

Electrochemical measurements

Electrochemical measurements of the $LiFePO_4$/C composites were accomplished by assembling CR2032 coin cells. The electrodes were made by dispersing the $LiFePO_4$/C composites, super-p carbon black, and an aqueous binder LA132 (Indigo, China) homogeneously in a weight ration of 80:10:10, casting the mixture uniformly onto an aluminum foil, and drying at 100 °C. All electrodes were punched in the form of a disk with a diameter of 14.5 mm (area of 1.65 cm^2), pressed, dried at 100 °C under vacuum for 8 h, and then weighed to determine the active mass. A typical electrode disk contained 4–5 mg cm^{-2} of $LiFePO_4$/C active material with a thickness of 350–400 μm when coated on aluminum foil.

The electrochemical performances of the $LiFePO_4$/C composites were evaluated with a lithium metal foil as the counter electrode and Celguard 2400 as the separator. The cell assembly was carried out in an argon-filled dry box. The electrolyte used was 1 mol L^{-1} $LiPF_6$ solution in a mixture of ethylene carbonate, dimethyl carbonate, and ethylene methyl carbonate (1:1:1 by volume). The cell was tested on a Neware Battery Tester (China) between 2.5 and 4.3 V, using a constant current charge/discharge mode. Cyclic voltammetry measurements were performed using an Arbin Instrument (USA) at a scan rate of 0.1 mV s^{-1} between 2.5 and 4.3 V (vs. Li/Li^+). Electrochemical impedance spectra were measured by using a Solatron 1260 Impedance Ananlyzer in the frequency range from 0.1 to 10^6 Hz at the open circuit with an ac voltage signal of 5 mV. All the tests were performed at room temperature.

Results and discussion

Influence of different carbon sources on properties of $LiFePO_4$/C composites

XRD, SEM, BET, and particle size distribution analysis

Figure 1 shows the XRD patterns of as-prepared $LiFePO_4$/C composites derived from different carbon sources. The XRD patterns reveal that both samples are single phase of $LiFePO_4$ which can be indexed to the orthorhombic olivine-type structure (JCPDS file no. 83–2092). It was

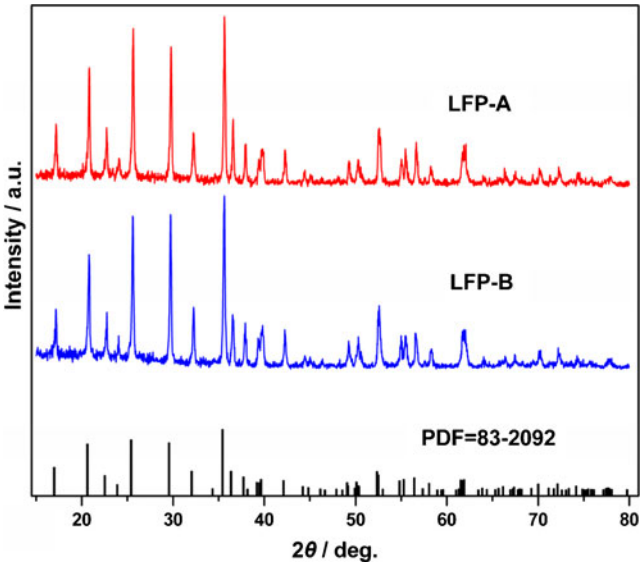

Fig. 1 XRD patterns of $LiFePO_4$/C composites derived from different carbon source

found that no impurities exist in the XRD patterns, suggesting that the carbon may avoid the appearance of impurity phase during the heat treatment. The lattice parameters of $LiFePO_4$/C composites are listed in Table 1. It shows that the lattice constants of the samples are approximately similar, indicating that the addition of different carbon sources has no obvious effect on the crystal structure of $LiFePO_4$ itself. There is no obvious diffraction response of the carbon because of its low content or amorphous state. The carbon content of the samples is listed in Table 2.

Figure 2 presents the SEM images of the precursors derived from different carbon sources. It can be observed that Fig. 2a has better uniformity in size distribution than Fig. 2b, indicating that PAALi, which has polymer frame, can improve the dispersion degree. The dispersion uniformity of the precursor can directly affect the particle size distribution of the final sample. The SEM images of $LiFePO_4$/C derived from different carbon sources are illustrated in Fig. 3. It can be seen that the sample LFP-A shows better particle size distribution than the sample LFP-B. The reason for this could be that the PAALi, which has polymer frame and viscosity, can inhibit the growth of the particle and enhance the dispersion degree, which is in good agreement with Fig. 2. It also can be found that the sample LFP-A

Table 1 The lattice parameters of the $LiFePO_4$/C composites obtained from different carbon sources

Sample ID	*a* (Å)	*b* (Å)	*c* (Å)	Cell volume (Å^3)
LFP-A	10.330	6.003	4.699	291.4
LFP-B	10.338	6.006	4.695	291.5
PDF=83-2092	10.334	6.010	4.693	291.5

Table 2 Powder properties of the $LiFePO_4$/C composites derived from different carbon sources

Sample ID	Carbon source	Carbon content (wt.%)	Specific surface area (g cm^{-2})	Particle size *D*50 (μm)
LFP-A	PAALi	4.11	24.7	1.86
LFP-B	Sucrose	4.32	17.4	3.25

derived from PAALi has plenty of nano-sized microstructure on the surface of the particles and the sample LFP-B derived from sucrose shows a comparatively glossy surface. The data from the BET measurement and laser particle analyzer are listed in Table 2. The sample LFP-A has larger

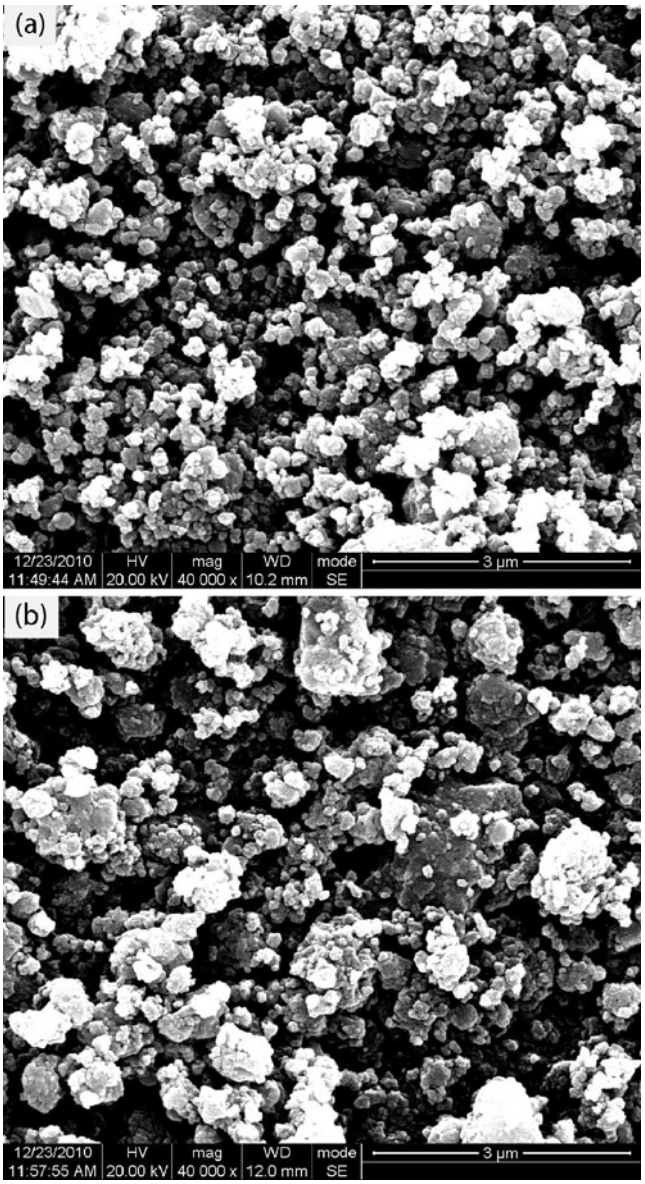

Fig. 2 SEM images of the precursors: **a** LFP-A, **b** LFP-B

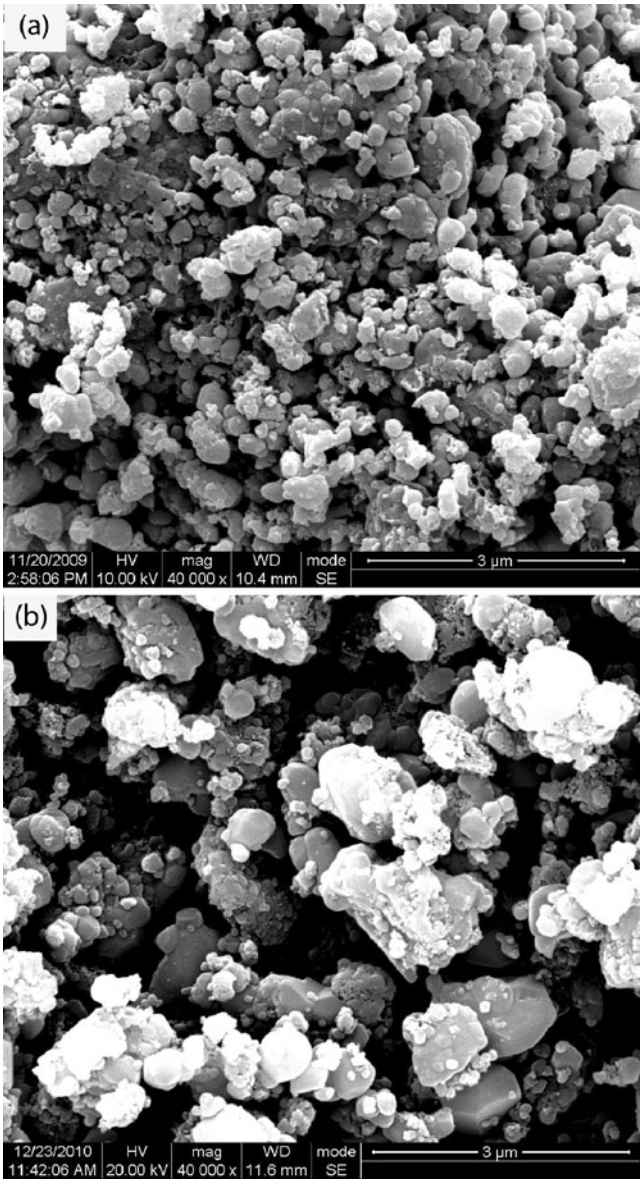

Fig. 3 SEM images of $LiFePO_4$/C composites: **a** LFP-A, **b** LFP-B

specific surface area and smaller particle size (*D*50) than LFP-B, and the results correspond with Fig. 3.

Raman spectroscopy analysis

Raman spectroscopy is a particularly useful tool for characterizing the structure of the carbon coating layer on the particles surface. Figure 4 and Table 3 display the Raman spectra of the composites in the range of 1,100–1,850 cm^{-1}. The group of peaks observed in the range of 1,530–1,640 and 1,250–1,450 cm^{-1} can be assigned to the graphite band (G-band), a disorder band (D-band), respectively. The G band corresponds to one of the E_{2g} modes, which has been assigned as the sp^2 graphite-like structure, whereas the D band corresponds to one of the A_{1g} modes, which is

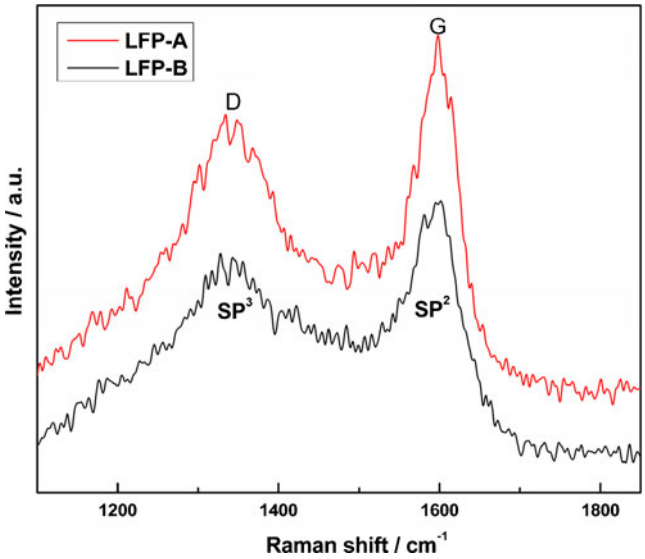

Fig. 4 Raman spectra of $LiFePO_4$/C composites obtained from different carbon sources

attributed to the sp^3 type tetrahedral carbon. The value I_D/I_G (the peak intensity ratio) can be used to evaluate the content of sp^3- and sp^2-coordinated carbon in the sample, as well as the degree of disorder for the pyrolytic carbon. Theoretically, higher relative intensity ratios of D/G correspond to a lower degree of order [32, 33]. It is reported that olivine $LiFePO_4$ with low I_D/I_G ratios outperformed good electrochemical properties [34]. So, PAALi is assumed to be a good additive to improve the character of $LiFePO_4$.

CVs analysis

Figure 5 shows the first cyclic voltammograms of the $LiFePO_4$/C cathode material derived from different carbon sources. As shown in Fig. 5, a single pair of well-defined redox peaks is observed for both samples. It suggested that there were no impurities in the composites, corresponding with the XRD patterns. The anodic and cathodic peaks correspond to the two-phase charge–discharge reaction of the Fe^{2+}/Fe^{3+} redox couple. The voltage separation (ΔV) between the anodic and the cathodic peaks is related to the polarization of the cell system, and the voltage separation (ΔV) between the anodic and the cathodic peaks of the same cycle is correlated to the polarization or reversibility of the redox reaction: the smaller the ΔV, the lower the polarization

Table 3 Raman spectra peak intensity and I_D/I_G ratio of samples derived from different carbon sources

Sample ID	Raman peak (cm^{-1})	I_D/I_G ratio
LFP-A	sp^3 1343 sp^2 1598	0.79
LFP-B	sp^3 1341 sp^2 1597	0.81

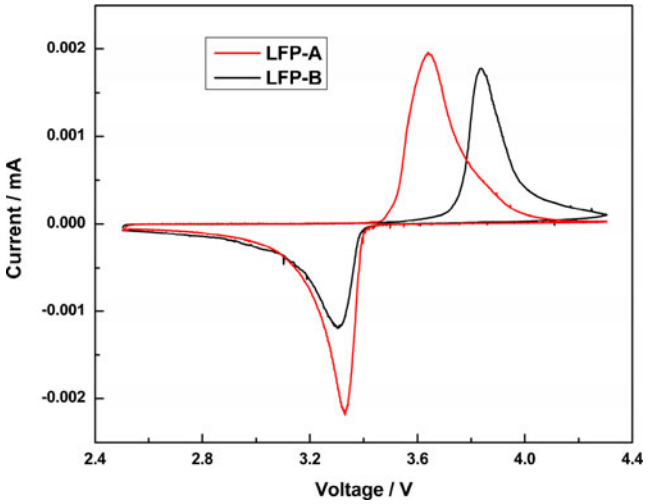

Fig. 5 First CVs of $LiFePO_4$/C composites derived from different carbon sources

or the greater the reversibility. In turn, this leads to greater cycle stability. From Fig. 5, we can see that the voltage separation (ΔV) between the anodic and the cathodic peaks are 0.31 and 0.52 V for the LFP-A and LFP-B, respectively, and the discharge peak currents decrease from LFP-A to LFP-B. Furthermore, LFP-A shows a smaller half-peak width than LFP-B. The above results indicates that the sample LFP-A has lower polarization and greater cycle stability.

Electrochemical analysis

The initial charge/discharge curves of $LiFePO_4$/C composites derived from different carbon sources are illustrated in Fig. 6 (a). It was found that the discharge capacities of LFP-A and LFP-B are 151 and 139 mAh g^{-1}, respectively. The coulomb efficiencies of $LiFePO_4$/C composites decrease from LFP-A to LFP-B. The higher discharge capacity and coulomb efficiency of the sample LFP-A can be explained in terms of fine particle size, low polarization, and resistance.

The cycle performance of the samples at a rate of 0.2 C is shown in Fig. 6 (b). It can be seen that the discharge capacity of the sample LFP-A gradually increases with the number of cycling, but the discharge capacity of the sample LFP-B firstly increases and then has slightly decreased. The capacity retentions are 104.5 % and 98.4 % for the samples LFP-A and LFP-B, respectively, after 50 cycles. The reasons for the differences can be attributed to the particle size, polarization, and internal resistance of the cells.

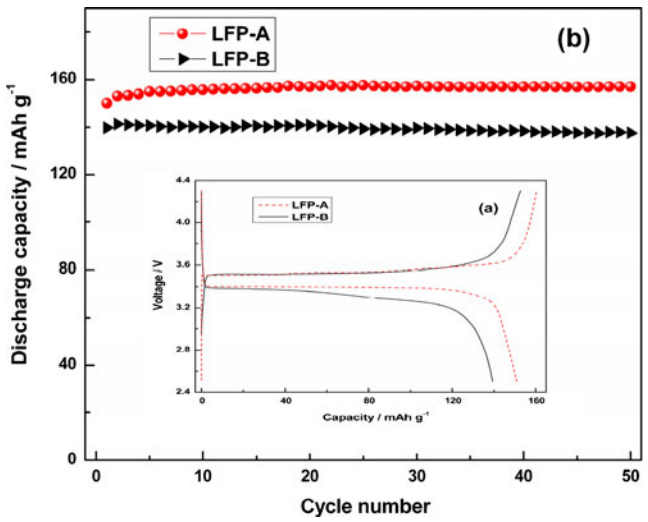

Fig. 6 Initial charge/discharge and cycling performances curves of $LiFePO_4$/C composites derived from different carbon sources at a rate of 0.2 C

EIS analysis

In order to understand in detail the influence of different carbon sources on the materials, electrochemical impedance spectra (EIS) measurements were carried out in a fresh coin cell as shown in Fig. 7. An intercept at the Z' axis in high frequency corresponded to the ohmic resistance (R_e), which represented the resistance of the electrolyte. The semicircle in the middle frequency range indicated the charge transfer resistance (R_{ct}). The inclined line in the low frequency range represented the Warburg impedance (Z_w), which was associated with lithium-ion diffusion in the $LiFePO_4$ particles. A simplified equivalent circuit model (Fig. 8) was constructed to analyze the impedance spectra. A constant phase element was placed to represent the double-layer capacitance and passivation film capacitance.

The lithium-ion diffusion coefficient could be calculated using the following equation [35]:

$$D = R^2T^2/2A^2n^4F^4c^2\sigma^2 \quad (1)$$

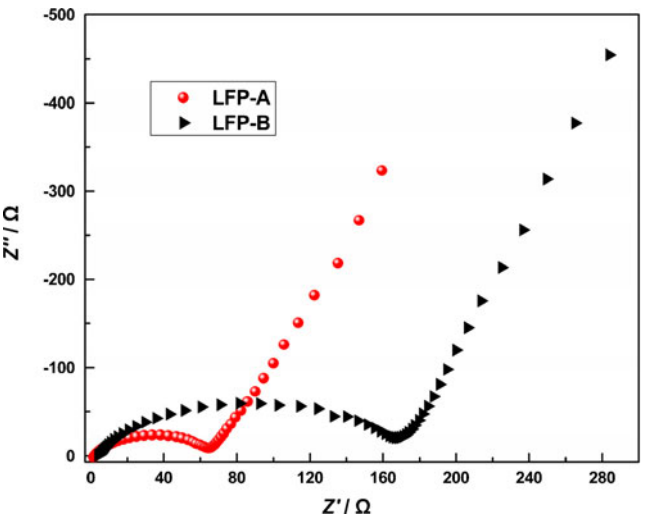

Fig. 7 Electrochemical impedance spectra of $LiFePO_4$/C composites from different carbon sources

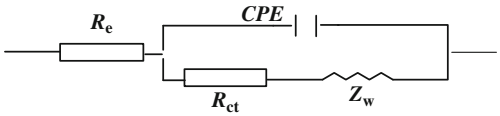

Fig. 8 Equivalent circuit used for fitting the experimental EIS data

Herein, R is the gas constant, T is the absolute temperature, A is the surface area of the cathode, n is the number of electrons per molecule during oxidization, F is the Faraday constant, C is the concentration of lithium-ion (7.69×10^{-3} mol cm^{-3}), and σ is the Warburg factor which is associated with Z_{re}.

$$Z_{re} = R_e + R_{ct} + \sigma\omega^{-1/2} \quad (2)$$

where ω is frequency. Figure 9 shows the relationship plot between Z_{re} and the reciprocal square root of the angular frequency ($\omega^{-1/2}$) at low frequency region. All the parameters obtained and calculated from EIS are shown in Table 4. It can be seen that the LFP-A has higher exchange current density ($i = RT/nFR_{ct}$) [36] and lithium-ion diffusion coefficient and lowest R_{ct} than LFP-B. It has been recognized that the middle frequency semicircle might correspond to the charge transfer impedance (R_{ct}) that resulted from the electrochemical reaction at the electrolyte and active material interface. The lower resistance of the sample LFP-A can be attributed to the abundance of nano-sized microstructure on the surface of the particles as the presence of such microstructures on the surface can aid the active material in effectively absorbing the electrolyte and thus accelerate the rate of electrochemical reaction on the interface. Meanwhile, lower polarization and fine particle size can also be propitious to decrease the resistance of sample, therefore enhancing the electrochemistry performances of LFP-A. This is consistent with the results in Figs. 4, 5, and 6.

Table 4 The impedance parameters of $LiFePO_4$/C composites obtained from different carbon sources

Sample ID	Re (Ω)	R_{ct} (Ω)	σ (Ω cm S$^{-1/2}$)	D (cm^2 S^{-1})	I (mA cm^{-2})
LFP-A	1.92	64	38.6	1.48×10^{-13}	4.01×10^{-4}
LFP-B	3.51	168	49.3	9.05×10^{-14}	1.53×10^{-4}

The said results show that the physical and electrochemical performances of as-prepared $LiFePO_4$/C are influenced greatly by different carbon sources. In the samples prepared by two selected carbon sources, LFP-A has a smaller particle size, bigger specific surface area, and lower I_D/I_G ratio, polarization, and internal resistance, which causes the better discharge capacity and cycling stability. The carbon content is another important influential factor on the electrochemical performances of $LiFePO_4$/C. Therefore, the effects of the carbon content on the electrochemical performance of LFP-A sample were systematically studied.

Influence of different carbon contents on the electrochemical properties of $LiFePO_4$/C

XRD analysis

The X-ray diffraction patterns of the samples containing different carbon contents are shown in Fig. 10. The XRD

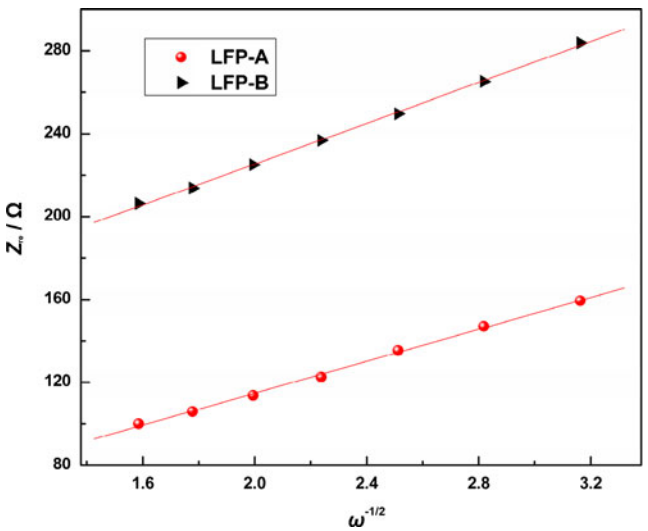

Fig. 9 The relationship plot between Z_{re} and $\omega^{-1/2}$ at the low-frequency region of the sample LFP-A and LFP-B

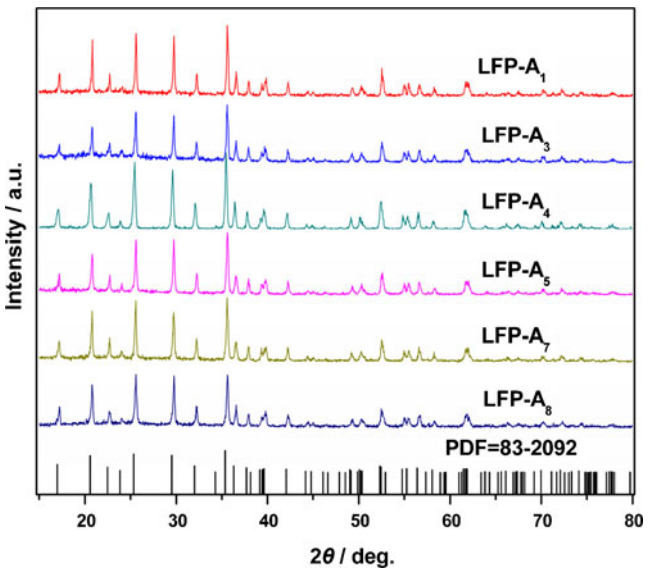

Fig. 10 XRD patterns of $LiFePO_4$/C composites with different carbon content

Table 5 The lattice parameters of the $LiFePO_4$/C composites with different carbon contents

Sample ID	*a* (Å)	*b* (Å)	*c* (Å)	Cell volume (Å^3)
LFP-A_1	10.335	6.010	4.695	291.6
LFP-A_3	10.333	6.005	4.691	291.1
LFP-A_4	10.335	6.005	4.695	291.4
LFP-A_5	10.330	6.003	4.699	291.4
LFP-A_7	10.325	6.013	4.698	291.7
LFP-A_8	10.340	5.999	4.697	291.3
PDF=83-2092	10.334	6.010	4.693	291.5

patterns show that olivine $LiFePO_4$ with an orthorhombic Pnma space group is the main crystalline phase in the samples. No impurities are detected in all the samples, which mean that olivine structure was maintained after our carbon coating process. The lattice parameters of $LiFePO_4$/C composites are listed in Table 5. It shows that the lattice constants of all the samples are approximately similar, indicating that the addition of different carbon content has no obvious effect on the crystal structure of $LiFePO_4$ itself. There is no obvious diffraction response of the carbon because of its low content or amorphous state. The carbon content of all the samples is listed in Table 6. From Table 6, we can also see that the tab density gradually decreases with increasing carbon content, and the discharge capacities of the samples firstly increases and then decrease. Hence, in order to obtain optimizing combination between tap density and discharge capacity, we should choose approximate carbon content. It can be found that LFP-A_5 (carbon content is 4.11 %) has optimum combination.

Electrochemical analysis

The cycling behavior of the samples containing different carbon content at a rate of 0.2 C is shown in Fig. 11. After 30 cycles, the capacity retention of LFP-A1, LFP-A2, LFP-A3, LFP-A4, LFP-A5, LFP-A6, LFP-A7, and LFP-A8 is 84.3, 103.7, 103.9, 103.6, 104.7, 104.1, 103.8, and 91.9 %, respectively. As shown in Fig. 11, the cycle performance of the samples LFP-A2, LFP-A3, LFP-A4, LFP-A5, LFP-A6, and LFP-A7 is better than LFP-A1 and LFP-A8 when there is a suitable carbon content. It is indicated that the added carbon of approximate amount enhances the intercalation reaction, reduces the surface polarization between electrode and electrolyte, and improves the cycle performance. However, when the carbon content is too low or too much, the cycle performance of the samples is poor. From Fig. 11, we can also see that when the carbon content is 4.11 % (molar ratio of PAALi/$Li_2C_2O_4$ is 2:1), the sample shows the best cycle performance and discharge capacity.

EIS analysis

To study in detail the influence of different carbon content on the materials, electrochemical impedance spectra measurements were carried out in a fresh coin cell as shown in Fig. 12. Figure 13 shows the relationship plot between Z_{re} and reciprocal square root of the angular frequency ($\omega^{-1/2}$) at low-frequency region. All the parameters obtained and calculated from EIS are shown in Table 7. It can be seen that the samples LFP-A2, LFP-A3, LFP-A4, LFP-A5, LFP-A6, and LFP-A7 have higher lithium-ion diffusion coefficient and exchange current density than LFP-A1 and LFP-A8 and lower R_{ct}. Furthermore, we can see that LFP-A5 has the highest lithium-ion diffusion coefficient and exchange current density and the lowest R_{ct}. We have discussed earlier that high lithium-ion diffusion coefficient and exchange current density and low R_{ct} can enhance the electrochemistry performance of the samples. Hence, the outcomes obtained from EIS analysis are consistent with the results in Fig. 11.

It is evident in the said results that the electrochemical properties of $LiFePO_4$ are correlated to carbon

Table 6 Carbon contents, tap densities, and initial discharge capacities of $LiFePO_4$/C composites prepared by different molar ratios of PAALi/$Li_2C_2O_4$

Sample ID	Molar ratio (PAALi/$Li_2C_2O_4$)	Carbon content (wt.%)	Tap density (g cm^{-3})	Initial discharge capacity (mAh g^{-1})
LFP-A_1	1:4	1.21	1.19	133
LFP-A_2	1:3	1.81	1.18	134
LFP-A_3	1:2	2.32	1.17	133
LFP-A_4	1:1	3.04	1.15	136
LFP-A_5	2:1	4.11	1.15	151
LFP-A_6	3:1	4.21	1.13	140
LFP-A_7	4:1	4.84	1.06	137
LFP-A_8	All PAALi	6.67	0.96	136

The charge–discharge rate is 0.2 C

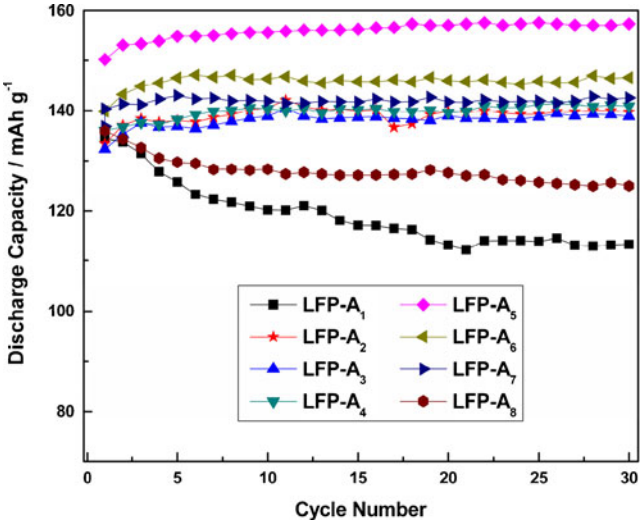

Fig. 11 Cycling performances of $LiFePO_4$/C composites containing different carbon content

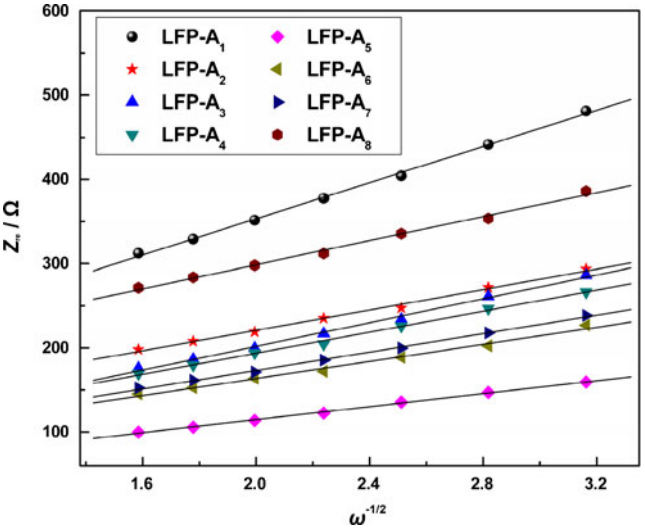

Fig. 13 The relationship plot between Z_{re} and $\omega^{-1/2}$ at the low-frequency region of the sample with different carbon content

content. It was known that carbon coating of the $LiFePO_4$ particle can possess an increase of the conductive connection, and the decrease of the $LiFePO_4$ particles can shorten the diffusion path of Li^+, which can all promote electrochemical performance. However, when the carbon content is too low, it is hard to form an integrated carbon coating network around the $LiFePO_4$ particle, which shows the bad electrochemical performance. When the carbon content is increased, the inactive carbon reduced the ratio of the active material, leading to a decrease in capacity. In addition, the carbon coating network is an intrinsically inert material for Li^+ storage, hindering Li^+ diffusion and resulting in a decrease in discharge capacity. Therefore, the $LiFePO_4$/C composite with approximate carbon content can display optimum performances.

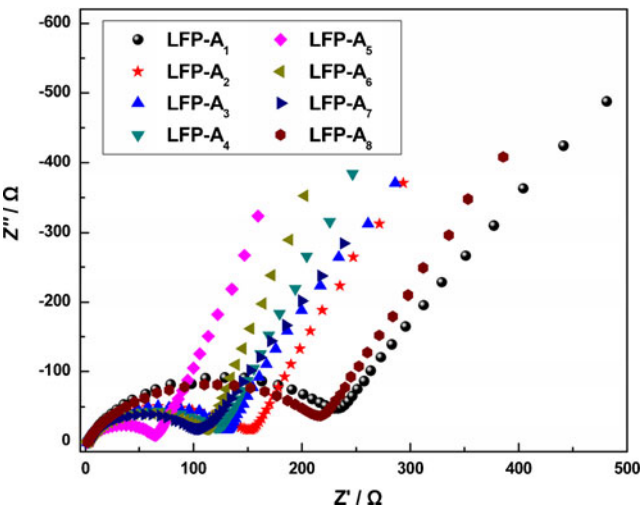

Fig. 12 Electrochemical impedance spectra of $LiFePO_4$/C composites with different carbon content

Conclusions

Two types of carbon source were employed to prepare the $LiFePO_4$/C composite: one using polymer (PAALi) and the other using sucrose. In our work, the results showed that PAALi was the better carbon source for the synthesis of $LiFePO_4$/C composite. Furthermore, the effects of carbon content on the performance of $LiFePO_4$/C were also investigated. The results demonstrate that as-prepared $LiFePO_4$/C composite showed the best combination between electrochemical performance and tap density when the carbon content is 4.11 wt.%.

Table 7 The impedance parameters of $LiFePO_4$/C composites with different carbon contents

Sample ID	*Re* (Ω)	R_{ct} (Ω)	σ (Ω cm S$^{-1/2}$)	D (cm^2 S^{-1})	I (mA cm^{-2})
LFP-A$_1$	2.63	230	107.4	1.91×10^{-14}	1.12×10^{-4}
LFP-A$_2$	4.23	151	60.7	5.97×10^{-14}	1.70×10^{-4}
LFP-A$_3$	2.28	130	70.6	4.41×10^{-14}	1.98×10^{-4}
LFP-A$_4$	3.11	122	62.5	5.63×10^{-14}	2.11×10^{-4}
LFP-A$_5$	1.92	64	38.6	1.48×10^{-13}	4.01×10^{-4}
LFP-A$_6$	1.87	110	50.8	8.52×10^{-14}	2.33×10^{-4}
LFP-A$_7$	2.77	108	54.8	7.33×10^{-14}	2.37×10^{-4}
LFP-A$_8$	2.47	218	71.3	4.33×10^{-14}	1.18×10^{-4}

Acknowledgment We gratefully acknowledge the support of the National High-Tech Research and Development Program of China (863 program, NO. 2009AA03Z231) and Chengdu Zhongke Laifang Energy and Technology Co. Ltd.

References

1. Padhi AK, Nanjundaswamy KS, Goodenough JB (1997) J Electrochem Soc 144:1188–1194
2. Huang H, Yin SC, Nazar LF (2001) Electrochem Solid-State Lett 4:A170–A172
3. Prosini PP, Carewska M, Scaccia S, Wisniewski P, Passerini S, Pasquali M (2002) J Electrochem Soc 149:A886–A890
4. Barker J, Saidi MY, Swoyer JL (2003) Electrochem Solid-State Lett 6:A53–A55
5. Ellis BL, Makahnouk WRM, Makimura Y, Toghill K, Nazar LF (2007) Nat Mater 6:749–753
6. Shim J, Striebel KA (2003) J Power Sources 119–121:955–958
7. Myung ST, Komaba S, Hirosaki N, Yashiro H, Kumagai N (2004) Electrochim Acta 49:4213–4222
8. Amine K, Liu J, Belharouak I (2005) Electrochem Commun 7:669–673
9. Hu Y, Doeff MM, Kostecki R, Finones R (2004) J Electrochem Soc 151:A1279–A1285
10. Anderesson AS, Thomas JO (2001) J Power Sources 97–98:498–502
11. Croce F, Epifanio AD, Hassoun J, Deptula A, Olczac T, Scrosati B (2002) Electrochem Solid State Lett 5:A47–A50
12. Park KS, Son JT, Chung HT, Kim SJ, Lee CH, Kang KT, Kim HG (2004) Solid State Commun 129:311–314
13. Yamada A, Chung SC, Hinokuma K (2001) J Electrochem Soc 148:A224–A229
14. Mi CH, Zhao XB, Cao GS, Tu JP (2005) J Electrochem Soc 152: A483–A487
15. Shin HC, Park SB, Jang H, Chung KY, Cho WI (2008) Electrochim Acta 53:7946–7951
16. Chung SY, Bloking JT, Chiang YM (2002) Nat Mater 1:123–128
17. Wang D, Li H, Shi S, Huang X, Chen L (2005) Electrochim Acta 50:2955–2958
18. Wang Y, Cao G (2008) Adv Mater 20:2251–2269
19. Kim JK, Choi JW, Chauhan GS, Ahn JH, Hwang GC, Choi JB, Ahn HJ (2008) Electrochim Acta 53:8258–8264
20. Zaghib K, Shim J, Guerfi A, Charest P, Striebel KA (2005) Electrochem Solid-State Lett 8:A207–A210
21. Dominko R, Bele M, Gaberscek M, Remskar M, Hanzel D, Pejovnik S, Jamnik J (2005) J Electrochem Soc 152:A607–A610
22. Charles RS, Fausto C, Vaneica YY, Charles RM, Bruno S (2005) Electrochem Solid-State Lett 8:A484–A485
23. Cui G, Hu YS, Zhi L, Wu D, Lieberwirth I, Maier J, Müllen K (2007) Small 3:2066–2069
24. Cui G, Gu L, Zhi L, Kaskhedikar N, Aken PAV, Müllen K, Maier J (2008) Adv Mater 20:3079–3083
25. Wang GX, Yang L, Chen Y, Wang JZ, Bewlay S, Liu HK (2005) Electrochim Acta 50:4649–4954
26. Fedorková A, Nacher-Alejos A, Gómez-Romero P, Oriňáková R, Kaniansky D (2010) Electrochim Acta 55:944–947
27. Huang YH, Park KS, Goodenough JB (2006) J Electrochem Soc 153:A2282–A2286
28. Park KS, Schougaard SB, Goodenough JB (2007) Adv Mater 19:848–851
29. Xia Y, Yoshio M, Noguchi H (2006) Electrochim Acta 52:240–245
30. Bauer EM, Bellitto C, Righini G, Pasquali M (2005) J Power Sources 146:544–549
31. Mestre-Aizpurua F, Hamelet S, Masquelier C, Palacín MR (2010) J Power Sources 195:6897–6901
32. Hiura H, Ebbesen TW, Tanigaki K, Takahashi H (1993) Chem Phys Lett 202:509–512
33. Bhuvaneswari MS, Bramnik NN, Ensling D, Ehrenberg H, Jaegermann W (2008) J Power Sources 180:553–560
34. Doeff MM, Wilcox JD, Kostecki R, Lau G (2006) J Power Sources 163:180–184
35. Jin B, Jin EM, Park KH, Gu HB (2008) Electrochem Commun 10:1539–1540
36. Shenouda Atef Y, Murali KR (2008) J Power Sources 176:332–339